

Article

Sedimentary Evolution and Geological Characteristics of the Jurassic in the South Qiangtang Basin, China

Zhanhu Cai ¹, Hong You ² and Qilin Wu ^{1,*}

¹ Department of Petroleum Engineering, Guangdong University of Petrochemical Technology, Maoming 525000, China

² Department of Chemical Engineering, Guangdong University of Petrochemical Technology, Maoming 525000, China

* Correspondence: wuqilin666@126.com

Abstract: Based on the analysis of lithology, lithofacies combinations, sedimentary structures, and fossil types in five geological sections measured through fieldwork, this paper comprehensively elucidates the sedimentary evolution characteristics of the Jurassic period in the South Qiangtang area. The South Qiangtang Basin is renowned for preserving the most complete Jurassic marine sedimentary strata in China, and it primarily consists of a mixed platform environment of carbonate and clastic rocks. The Jurassic strata in the South Qiangtang Basin range from the Quse Formation at the base to the Suowa Formation at the summit, with sedimentary facies evolving from the outer shelf to the subtidal zone, and seawater depth gradually becoming shallower. This trend may be associated with the division and expansion of the Bangong–Nujiang suture zone during the Late Triassic, subduction in the Middle Jurassic, and the suture and splicing of the Qiangtang–Lhasa plate during the Late Jurassic tectonic movements. In conclusion, this research presents a comprehensive analysis of the sedimentary evolution of the Jurassic period in the South Qiangtang Basin for the first time. The findings offer significant contributions to the understanding of the region’s geological history and serve as a valuable foundation for future investigations.

Keywords: Jurassic; Qiangtang Basin; sedimentary facies; sea-level change



Citation: Cai, Z.; You, H.; Wu, Q. Sedimentary Evolution and Geological Characteristics of the Jurassic in the South Qiangtang Basin, China. *Processes* **2023**, *11*, 1569. <https://doi.org/10.3390/pr11051569>

Academic Editors: Yinhui Zuo and Hui Han

Received: 26 March 2023

Revised: 18 May 2023

Accepted: 19 May 2023

Published: 21 May 2023



Copyright: © 2023 by the authors. Licensee MDPI, Basel, Switzerland. This article is an open access article distributed under the terms and conditions of the Creative Commons Attribution (CC BY) license (<https://creativecommons.org/licenses/by/4.0/>).

1. Introduction

In the 19th International Sedimentological Congress [1], the Triassic–Jurassic Basins within the Tethys region garnered significant attention, indicating a global interest in the Tethys domain. This domain is noteworthy, as it contains approximately 68% of the world’s hydrocarbon reserves. During the Jurassic period, the Alps, Apennines, and Sicily underwent significant geological transformations, driven by the breakup of the supercontinent Pangaea and the expansion of the Tethys Ocean [2–4]. The evolution of these regions was marked by the formation of new basins, mountain-building events, and the deposition of sediments that preserved a rich record of Jurassic life [5]. The formation of the Alps started during the Jurassic period, as the African Plate began to move northward, converging with the Eurasian Plate. During this time, the Tethys Ocean, which separated the two plates, began to shrink. The sediments deposited in the shallow marine environments along the margins of the Tethys Ocean formed the basis for the future Alpine mountain range. The ongoing plate convergence throughout the Jurassic and subsequent periods led to the uplift and folding of these sediments, eventually forming the high peaks of the Alps. The rich fossil record found in the Jurassic limestones of the Alps provides important information on the marine life that thrived in the Tethys Ocean [6]. During the Jurassic period, the region was part of the southern margin of the Tethys Ocean. As the African Plate moved northward, it began to collide with the Eurasian Plate, causing the formation of the Apennine Mountain range. Jurassic sediments deposited in the region include marine limestones, which contain fossils of various marine organisms, such as ammonites, bivalves,

and corals [6]. During the Jurassic period, Sicily was located at the southern margin of the Tethys Ocean. The geological evolution of Sicily was influenced by the northward movement of the African Plate and the associated tectonic activity. Jurassic sediments in Sicily consist of shallow marine limestones and dolomites, which contain abundant fossils of marine organisms such as ammonites, belemnites, and brachiopods [7–9]. The deposition of these sediments laid the groundwork for the formation of the Sicilian Mountain ranges that emerged during subsequent geological periods.

The Tibetan region, which is located at the easternmost part of the Tethys domain, is distinguished by its extensive marine deposits in Northern Tibet (Figure 1), which are the largest in China [10]. Researchers have identified the Jurassic as the most comprehensive and widespread marine sedimentary system within the Qiangtang Basin of Northern Tibet [11–16].

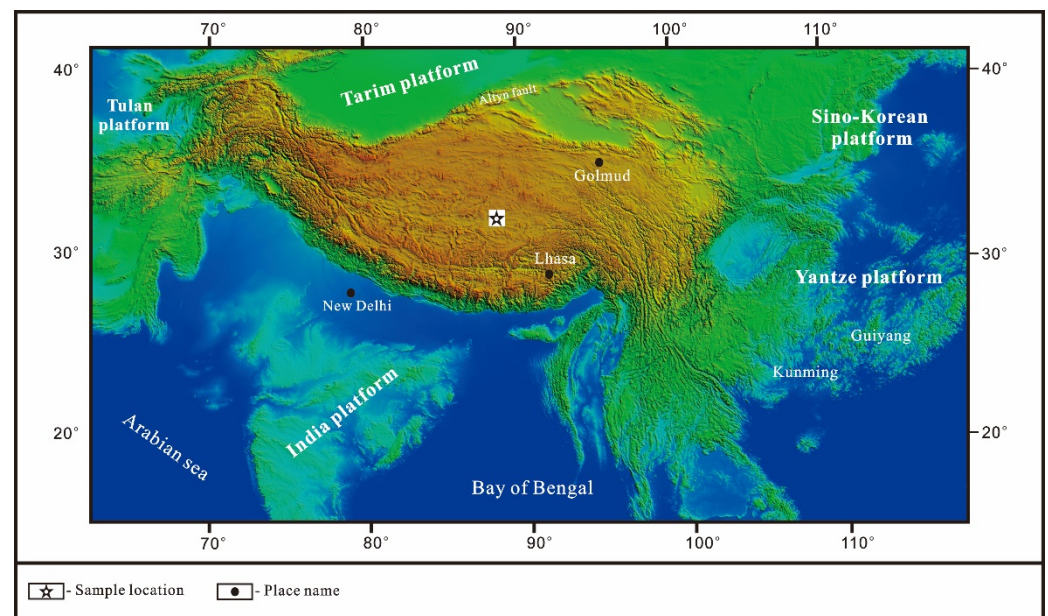


Figure 1. Regional tectonic location map of Qiangtang Basin.

During the Late Triassic, the Qiangtang Basin was formed through the amalgamation of two blocks: the Qiangnan–Baoshan from the northern margin of Gondwana and the Qiangbei–Changdu from Eurasia. The Longmucuo–Shuanghu suture zone divided this basin into two distinct sedimentary basins, namely the South Qiangtang and North Qiangtang. It is important to note that seawater intrusion only transpired within both basins during the Bajocian and Oxfordian periods [17–24]. Establishing a well-developed lithostratigraphic system is essential for conducting geological research.

Although numerous studies have been conducted on rock stratigraphy, biostratigraphy, geochemical stratigraphy, and physical stratigraphy in the South Qiangtang Basin, a comprehensive investigation of the sedimentary evolution of the Jurassic system in this region has yet to be undertaken.

2. Geological Setting

The Qiangtang Basin, centrally positioned within the Tethys–Himalayan orogenic belt, stretches from the Kekexili–Jinsha suture zone in the north to the Bangong–Nujiang suture zone in the south. As the second-largest marine sedimentary basin in China, it can be subdivided into five secondary tectonic units based on stratigraphic distribution, sedimentary characteristics, tectonic deformation, magmatic activity, and regional comparisons. These units include the Eastern Uplift, Western Uplift, Central Uplift, North Qiangtang Depression, and South Qiangtang Depression, displaying a block-like pattern from east to west and a belt-like pattern from north to south (Figure 2).

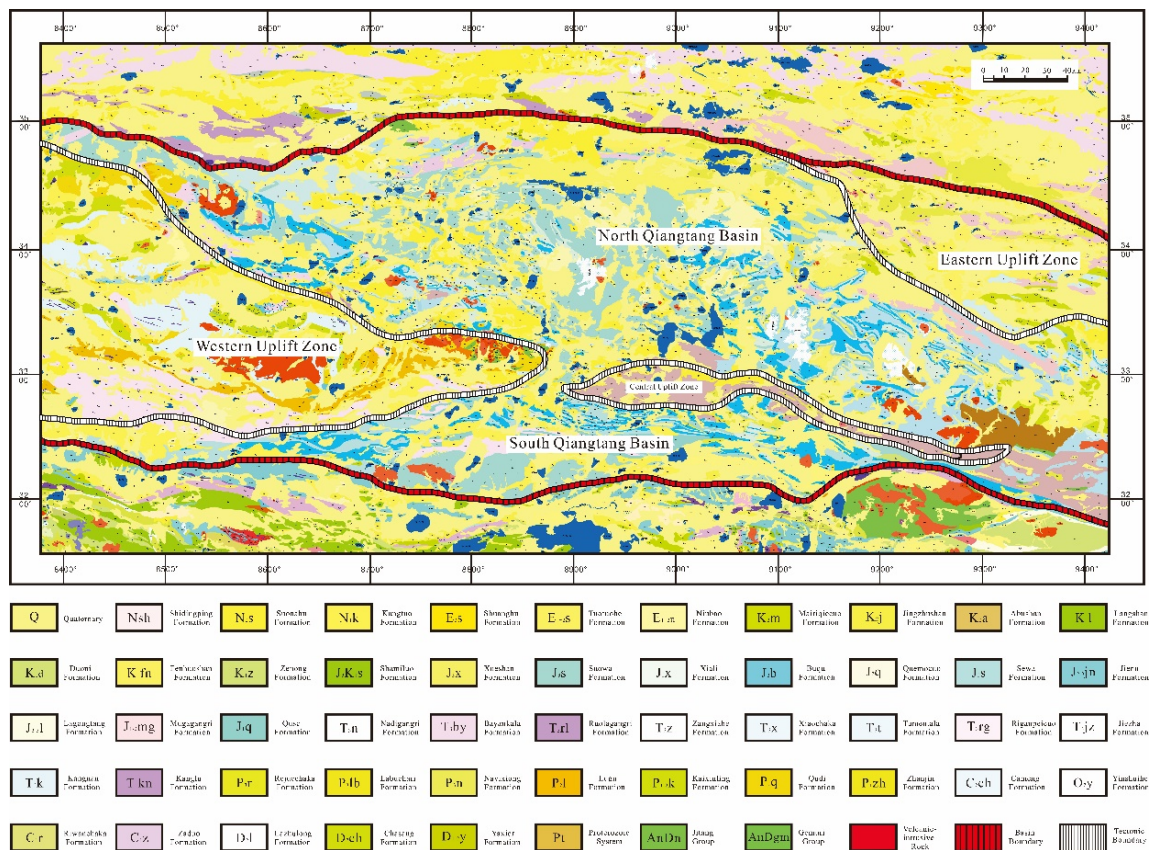


Figure 2. Zoning map of the Qiangtang Basin tectonic unit.

The study area, encompassing the South Qiangtang Depression, lies south of the Central Uplift Belt and is bordered by the Bangong–Nujiang suture zone to the south. This elongated east–west basin is characterized by preserved Middle and Cenozoic strata development, with the Jurassic system prominently developed in an east–west direction. Upper Middle Jurassic strata are primarily exposed near the Central Uplift Zone in the northern area, while Lower Middle Jurassic strata occupy a significant portion of the southern area. Based on a 1:250,000 regional geological survey by the Jilin Geological Survey Institute, six formations have been identified within the Jurassic stratigraphy, in ascending order: Quse Formation (J_{1q}), Sewa Formation (J_{2s}), Shaqiaomu Formation (J_{2sq}), Buqu Formation (J_{2b}), Xiali Formation (J_{2x}) and Suowa Formation (J_{3s}).

Despite the numerous studies on lithostratigraphy, biostratigraphy, geochemistry, and physical stratigraphy conducted over the past three decades, measured sections often display inaccuracies, low quality, and inconsistencies. Consequently, these issues have made comparative stratigraphic studies challenging. Furthermore, no researcher has thoroughly investigated the complete sedimentary evolution of all six Jurassic formations present in the South Qiangtang Basin. To address this gap, the author has analyzed five “shoe-and-hat” sections to explore their evolutionary characteristics.

3. Materials and Methods

To address this gap, we selected five Jurassic stratigraphic sections that exhibit complete sequences, distinct top–bottom boundaries, and abundant fossils for analysis. The selection was based on data from regional geological surveys and petroleum geological surveys conducted by previous researchers.

The five Jurassic stratigraphic sections measured in this study are: (i) Rugumiqiong section (RGS); (ii) Dongbulake section (DBS); (iii) Migaiertuoba section (MGS); (iv) Ganbeixiama section (GBS), and (v) Ganbeixiamanan section (GBNS). Three sections, namely

RGS, DBS, and MGS, are situated in the northern region of the South Qiangtang Basin. These sections are approximately 50 km south of the Shuanghu Special Administrative Region, located in the Dongbula Mountains (Figure 3a). These sections measure the Suowa Formation, Xiali Formation, and Buchu Formation. The remaining two sections, GBS and GBNS, are situated in the southern part of the basin, within the Ganbeixiama area. These sections are approximately 5 km south of Angdaercuo (Figure 3b). These sections measure the Shaqiaomu Formation, Sewa Formation, and Quse Formation.

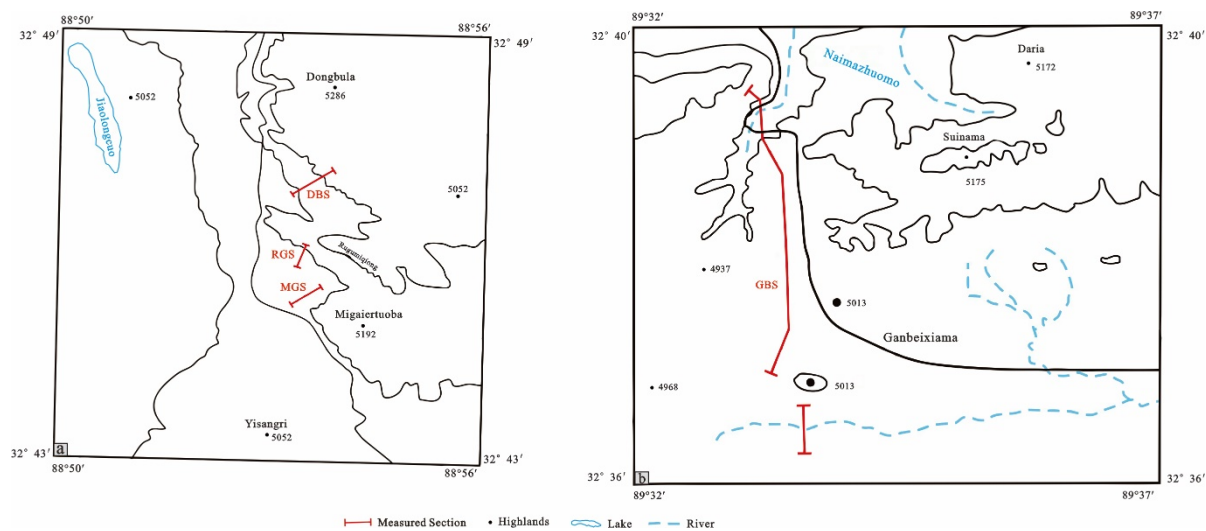


Figure 3. Location map of measured sections of Jurassic in Shuanghu County. (a) Surveying three sections of the Middle and Upper Jurassic; (b) Surveying two sections of the Lower Jurassic.

4. Results

The measured section plane has a total length of 6218 m and a cumulative true thickness of 3668.72 m. The thicknesses of the Suowa Formation, Xiali Formation, Buqu Formation, Shaqiaomu Formation, Sewa Formation, and Quse Formation are 78.8 m, 757.50 m, 342.08 m, 1080.65 m, 942.54 m, and 396.50 m, respectively. These six formations exhibit integrated contact with each other. Across the five sections, a total of 60 conductors were measured, and 772 samples were collected.

4.1. RGS

The section is situated on the southern slope of Rugumiqiong, extending from the summit to the base along a near north–south valley. The southern end of the section is covered by a substantial area of Quaternary deposits and can be connected to the top 21 layers of the RGS through a marker layer. In contrast, the northern end of the section is proximal to the summit of Mount Rugumiqiong and exhibits a distinct boundary with the Suowa Formation. The Suowa Formation comprises a large set of carbonate deposits that are geomorphologically upright and steeply cantilevered, resulting in an integrated contact between the two formations (Figure 4). The sections are enumerated below.

4.2. DBS

The section is located on the south flank slope of Dongbula backslope. The profile's starting point is at a mountain pass where two sets of tuff steep cans exit, displaying an evident geomorphic standard. The profile extends from the summit to the base along a near north–south valley. Its northeastern end exhibits integrated contact with the Buqu Formation, while its southwestern section is covered by a substantial area of Quaternary deposits. It can be connected to the bottom 20 layers of the DBS through a gray-green slate fine sandstone layer (Figure 5). The sections are enumerated below.

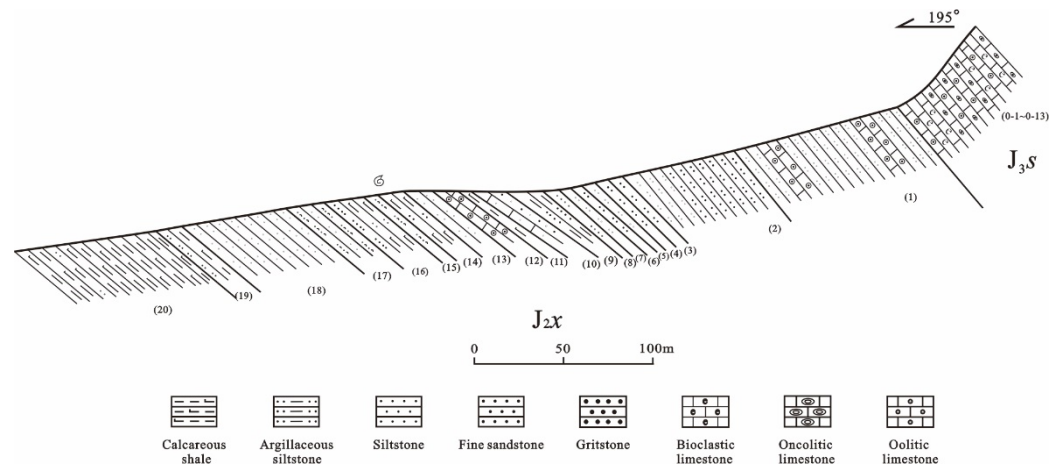


Figure 4. Field survey stratigraphic section of Rugumiqiong (MGS). The numbers in the figure are the sublayers when the section is measured.

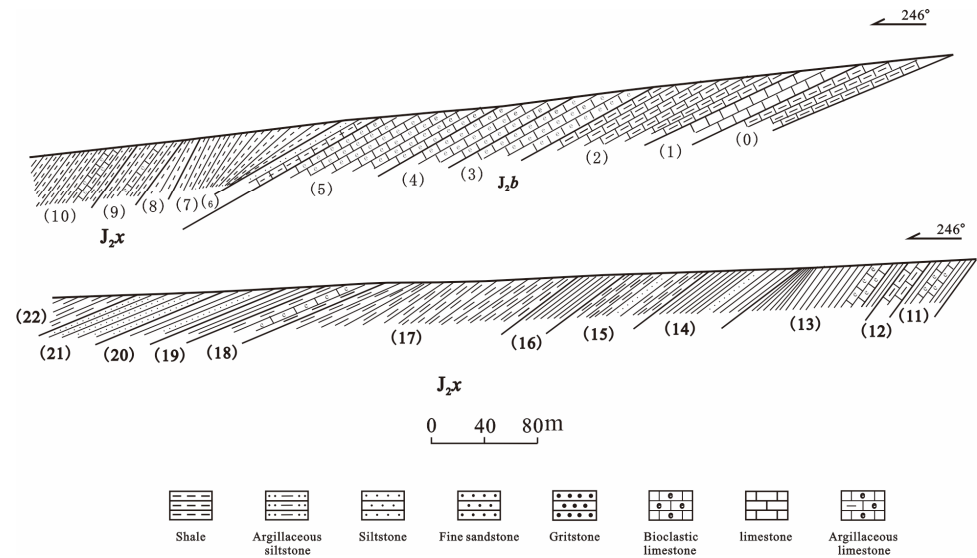


Figure 5. Field survey stratigraphic section of Dongbula (DBS). The numbers in the figure are the sublayers when the section is measured.

4.3. MGS

The section is situated on the southern slope of Migaiertuoba. The profile commences at Guogencuo Road adjacent to a valley and extends along a north–east measurement system. Its southwest end demonstrates integrated contact with the Shaqiaomu Formation, while its northeast end shows integrated contact with the Xiali Formation. The geomorphic standard is evident. The Buqu Formation comprises carbonate rocks that form ridges due to their positive topography, whereas the upper and lower sets of clastic rocks form negative topography resulting from weathering effects (Figure 6). The sections are enumerated below.

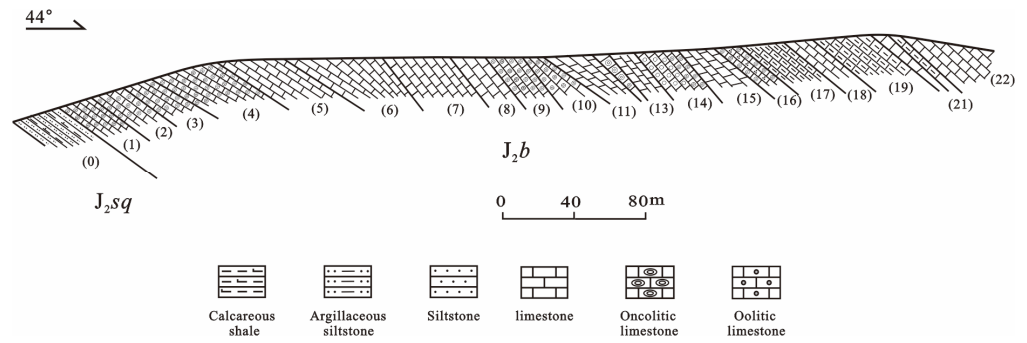


Figure 6. Field survey stratigraphic section of Migaiertuoba (MGS). The numbers in the figure are the sublayers when the section is measured.

4.4. GBS

The study area is situated on the northern flank of the Ganbeixiama compound dorsal oblique. The starting point of the section lies at the core of the dorsal oblique, featuring geomorphology that transitions from a high mountain in the south to a low valley in the north. The road direction shifts from a north–south orientation to an east–west one, tracing an east–west ditch at the core of the dorsal oblique. The outcrop exhibits exceptional quality. The encountered stratigraphy comprises the Suowa Formation, Shaqiaomu Formation, and Buqu Formation. The northwest end is in integrated contact with the Buqu Formation, demonstrating an evident geomorphic standard with orthogonal carbonate formation. The southeast end is positioned at the core of the Ganbeixiama backslope, with its base obscured (Figure 7). The sections are delineated as follows:

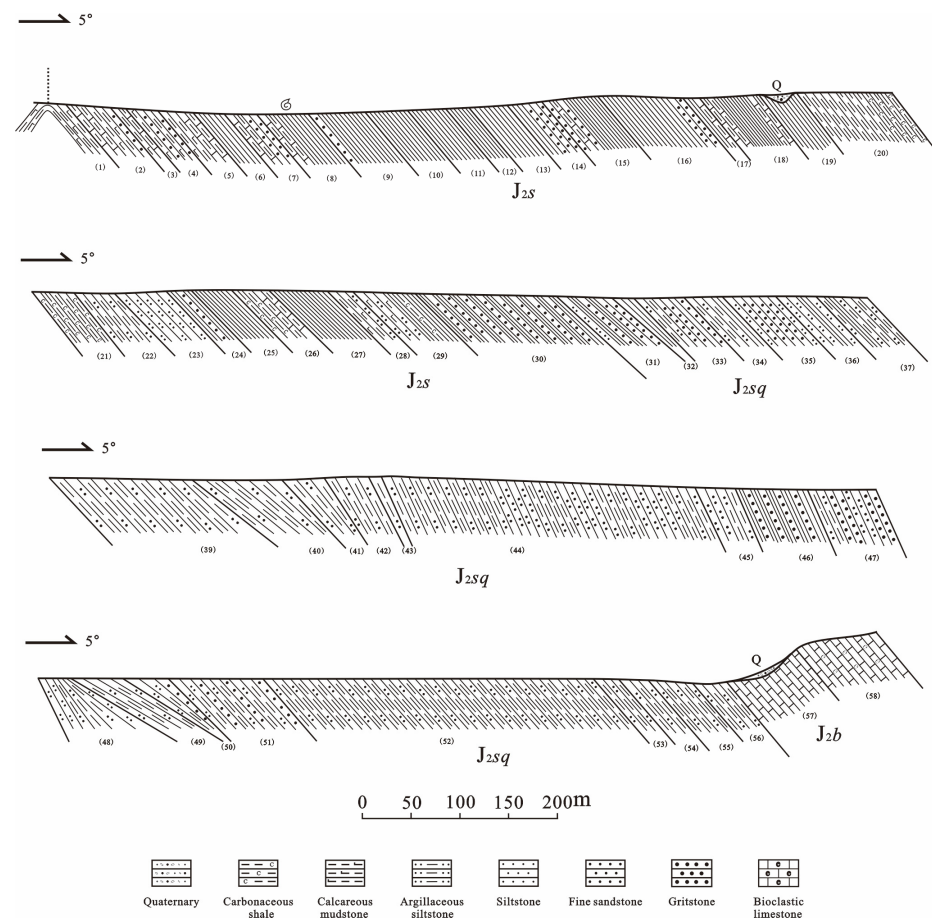


Figure 7. Field survey stratigraphic section of Ganbeixiama (GBS). The numbers in the figure are the sublayers when the section is measured.

4.5. GBNS

The section is located on the Ganbeixiama compound, extending to the back and oblique south. The starting point of the profile was selected in the oblique core section, which is geomorphologically situated south of Ganbeixiama mountain and presents a distinct geomorphological standard. The northern end of the profile resides within the core of the oblique section, while the southern end is concealed by plateau sand from the fourth system, leaving its top and bottom undisclosed (Figure 8). The section is described as follows:

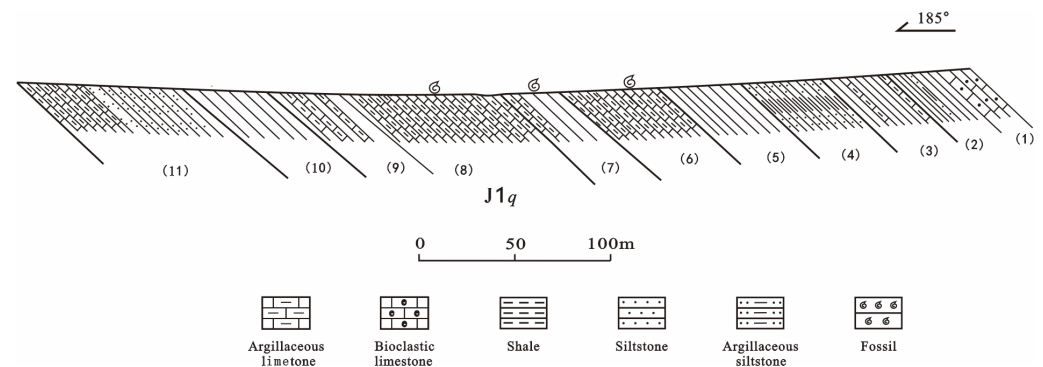


Figure 8. Field survey stratigraphic section of Migaiertuoba (GBNS). The numbers in the figure are the sublayers when the section is measured.

5. Discussion

A comprehensive sedimentary phase study was conducted through the observation and description of the measured stratigraphic sections, based on color, lithology, lithological assemblage characteristics, sedimentary tectonics, and the type of fossils contained. The sedimentary characteristics of each stratum are as follows:

5.1. Quse Formation (J_1q)

In the stratigraphic section of Ganbeixiama, the base is characterized by a substantial set of dark gray and gray-black mud shales, very thinly bedded and bladed, interbedded with a few thinly bedded siltstones and mud tuffs. The central part features thinly bedded and very thinly bedded shales and thinly bedded mud tuffs, interbedded in unequal thickness, locally with siltstones and siltstone interbedded in unequal thickness as well. The upper part is typified by a large set of grayish white mudstone outcrops. Four types of fundamental stratigraphic sequences can be observed (Figure 9), which include:

Type A: The bioclastic tuff, which is interbedded with marl, is located in layer 1 at the top of the section. This bioclastic tuff exhibits a grayish black hue and is thinly to moderately laminated. Individual layers typically range between 5 and 40 cm in thickness. In contrast, the marl is light gray, thinly laminated, and has single layers that are generally 5–10 cm thick. Chrysolitic and bivalve fossils are present within the marl. The thickness of individual sedimentary base sequences varies from 10 to 50 cm. The large numbers of thinly bedded bioclastic deposits may signify a storm genesis, which could indicate a shallow inland shelf zone near the offshore shore (Figure 10).

Type B: Unequal thicknesses of shale and marl interbedding characterize this type of base sequence, predominantly developed in the central part of the section. The shale is generally dark black, page-like, and easily weathers into mound-like and graveyard-like structures. The marl, on the other hand, is gray-black and thin-to-medium bedded. The thickness of a single layer typically varies from 5 to 20 cm. A few chrysolite-like biological fossils are occasionally observed. The thickness of the single base sequence ranges from 30 to 150 cm and is mainly developed in layers 3, 6, and 7 of the section. The stratigraphy is dominated by large sets of fine-grained sediments, locally interspersed with muddy tuffs, which are rich in chrysolite and benthic bivalve fossils with in situ burial characteristics.

The mudstone and shale rocks are generally black and dark gray in color and locally rich in pyrite nodules. This represents an anoxic, stagnant, and undercompensated confined basin or redox interface. Such rocks can evolve into high-quality source rock; many oil and gas exploration practices show that known large and medium-sized gas fields are closely related to the source rocks [25,26].

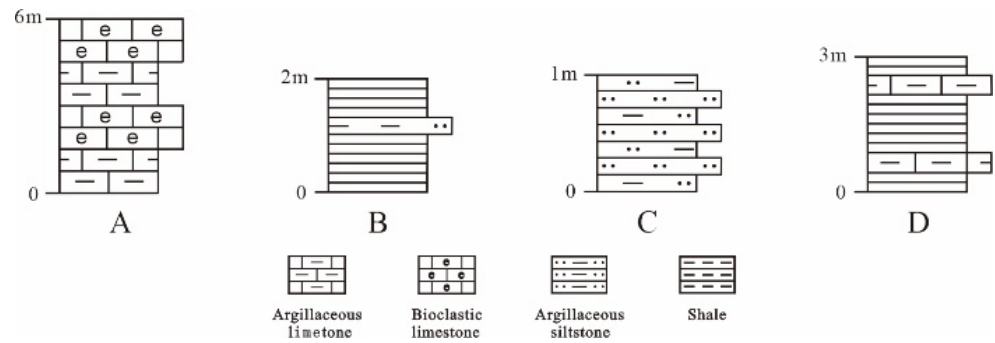


Figure 9. Stratigraphic sequence of the Quse formation. A, B, C, D are type A, type B, type C, type D respectively.

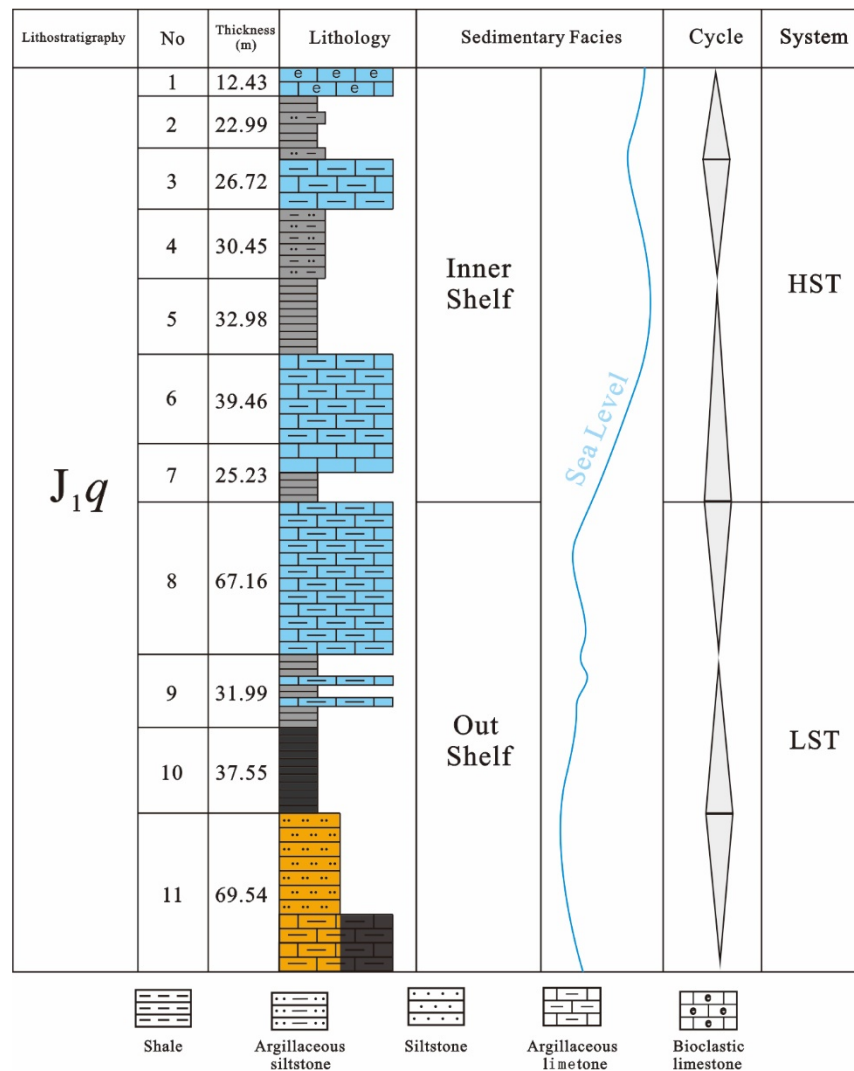


Figure 10. Sedimentary facies of the Quse formation. Sandstone is uniformly filled in yellow, and carbonate rock is uniformly filled in cyan.

Type C: Interbedded siltstone and siltstone mudstone are also widely distributed in the stratigraphy of the Quse Formation. The siltstone is typically gray or light gray, thinly bedded, with a single layer thickness generally around 5 cm and laterally rock-stable. The siltstone mudstone is dark gray or black, thinly bedded to very thin, and has a single layer thickness that generally varies from 1 to 5 cm. Local layers contain chrysolitic and bivalve fossils, which may represent an inland shelf sedimentary environment.

Type D: Shale interbedded with siltstone mudstone characterizes this type of base sequence, which is widely developed in the Quse Formation and serves as the primary base sequence. The shale is generally dark black, with shale flakes very wave-laminated, and the rocks are easily weathered to an earthy texture. The siltstone mudstone is light gray, has a single layer thickness of 1 to 3 cm, and exhibits a stable lateral extension. Large sets of shale occurrence may represent an offshore shelf depositional environment. The siltstone is typically thinly bedded and has a stable lateral extension, which may signify offshore shelf storm genesis deposition.

During the Toarcian period in the Alps, shallow marine facies played a prominent role in characterizing the depositional environments of the region. Composed of limestones, marls, and calcareous sandstones, these facies are indicative of shallow marine settings such as continental shelves and carbonate platforms. The presence of fossils, including bivalves, gastropods, and ammonites, suggests a warm, shallow sea with high biological productivity. Furthermore, sedimentary structures such as ripple marks, cross-bedding, and bioturbation are commonly observed, providing additional insight into the depositional processes that shaped these environments [27].

5.2. Sewa Formation (J_{2s})

In the analyzed stratigraphic section of Ganbeixiama, the Sewa Formation primarily consists of gray-black and dark gray shales (Figure 11A) and mud shales, interbedded with gray-black siltstones or muddy siltstones. Locally, gray-black fine sandstones (Figure 11B) are also present within the layers.

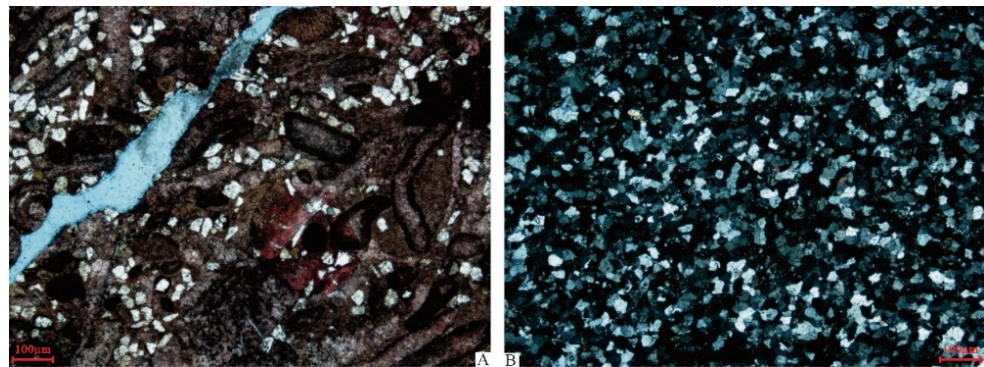


Figure 11. Microscopic photos of the rocks of the Sewa Formation ((A): Shale, (B): Fine sandstones).

Three distinct types of basic sequences can be observed (Figure 12), which are as follows:

Type A: This sequence is characterized by the interstratification of gray-black shale and mudstone. The shale generally presents in very thin laminae and phyllite sheets, with well-developed horizontal grain layers. The color is darker, and the organic matter content is higher. Occasionally, pyrite particles or nodules are visible, as well as lenticular or thin laminae gray-black marl interstratification in certain areas. A large number of brachiopod and chrysopod fossils can be found in the gray rock, which is well-preserved and primarily distributed along the layers, showcasing in situ burial ecological characteristics. This sequence represents a deep-water tranquil reduction environment below the wave base surface and the CCD (carbonate compensation depth) surface. Type A sequences are

commonly developed in the Sewa Formation, exemplified by strata 1, 3, 5–8, 17–21, and 26–27 within the section (Figure 13).

Type B: This sequence features gray-black shale interbedded with yellow-gray, thinly laminated muddy siltstone. The shale rocks are predominantly dark black, with very thin laminations and phylloclastic output, as well as horizontal lamination development. The muddy siltstone is mostly yellow-gray or light gray, exhibiting thinly laminated output and a single layer thickness of 5–10 cm, accompanied by horizontal and undulating lamination development. The presence of large sets of muddy sediments with ripple-laminated and horizontally laminated sandstone interbeds may indicate an outer shelf depositional environment, characterized by deeper waters but occasional storm-flow waves. Type B sequences are also relatively well-developed within the Sewa Formation strata, as seen in layers 2, 4, 16, 25, and 28 of the section.

Type C: In this sequence, gray-black fine sandstone and siltstone are interbedded with gray-black shale and mudstone, or several of them are interbedded together. The sandstone is consistently thinly bedded, with a single layer thickness of 2–5 cm. Type C sequences can be observed in layers 9–15, 22–24, 29, and 30 of the section.

The vertical profile exhibits an alternating superposition of inland shelves and outcrop shelves. Within these sequences, there is a development of phase sequences, such as storm deposition sequences, as well as the extensive development of small-scale phase sequences analogous to meter-scale cyclones. These small-scale sequences range from tens of centimeters to two meters in thickness and are products of autogenic deposition processes controlled by heterogenic mechanisms. These mechanisms are primarily the result of a combination of factors, such as sediment basement subsidence, absolute sea-level changes, and alterations in sediment accumulation rates. Consequently, they generate a high-frequency cyclonic change in the depositional environment, characterized by deepening and shallowing phases. Autogenic mechanisms refer to changes such as the accretion of shoreline sands and channel migration.

In a wave-based, land-shelter sedimentation system, environmental deepening leads to the formation of fine-grained sediments, while shallowing results in the deposition of coarser sediments due to sand body accretion. The high-frequency periodic deepening and shallowing of the environment form several types of rhythmic cycles. The lower part of these cycles typically comprises mudstone and shale, while the upper part mostly consists of sandstone and siltstone units. Type A, characterized by “gray-black or black mud shale with gray or dark black mud shale”, and Type B, marked by “gray-black shale with thin yellow-gray laminated mud siltstone,” are primarily developed in the outer shelf phase zone. In contrast, Type C, which features “gray-black fine sandstone and siltstone interbedded with gray-black shale and mudstone”, is predominantly found in the inland shed phase zone.

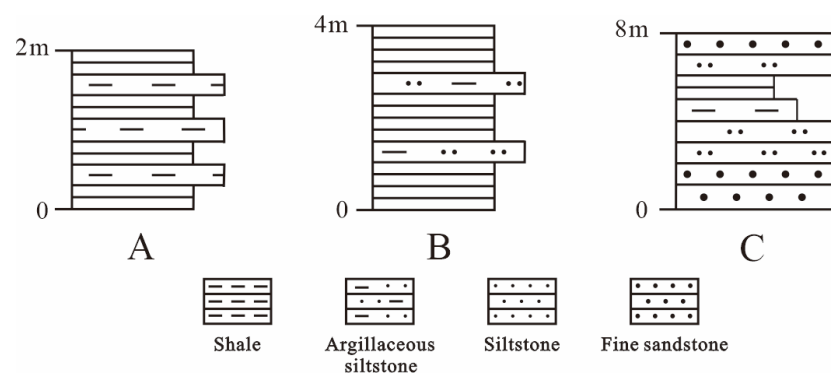


Figure 12. Stratigraphic sequence of the Sewa formation. A, B, C are type A, type B, type C respectively.

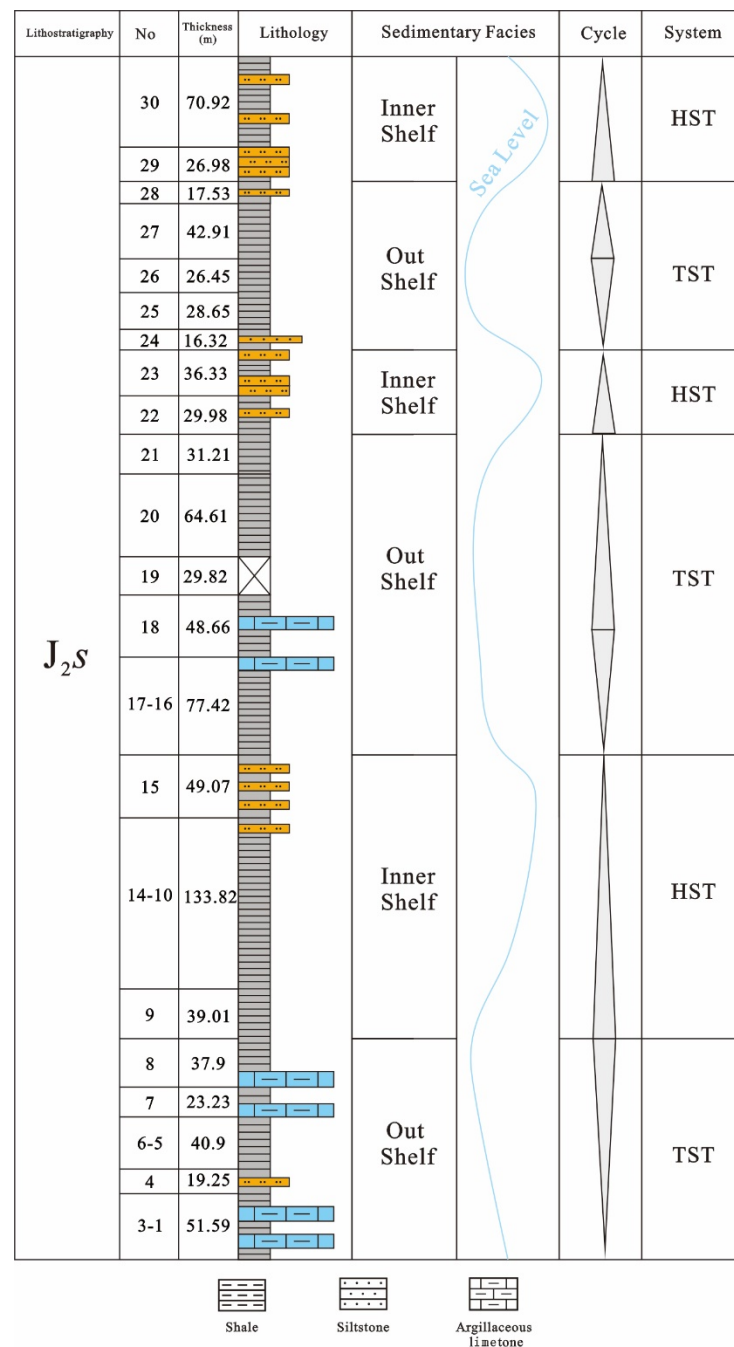


Figure 13. Sedimentary facies of the Sewa formation. Sandstone is uniformly filled in yellow, and carbonate rock is uniformly filled in cyan.

During the Bajocian period in the Alps, the shallow marine environments fostered the formation of sedimentary rocks, which predominantly consist of limestones, marls, and calcareous shales. These rocks are typically rich in calcium carbonate, originating from the shells and skeletons of the diverse marine organisms that inhabited these ecosystems. The abundance of fossils, such as ammonites, belemnites, bivalves, brachiopods, gastropods, and marine microfossils such as foraminifera and coccolithophores, found within the sedimentary rocks provides evidence for the variety of marine life that thrived during this period [28].

5.3. Shaqiaomu Formation ($J_2^{\hat{s}q}$)

In the Ganbeixiama section, the base primarily consists of a series of yellowish-brown and dark purple siltstone and fine sandstone layers, interspersed with gray and black siltstone, mudstone (Figure 14A), and shale. There are gouge marks and channel molding structures present in the sandstone. The middle and upper parts comprise a series of light gray, gray, and black siltstone (Figure 14B), mudstone, and shale layers, interspersed with gray-green and light gray siltstone and fine sandstone.

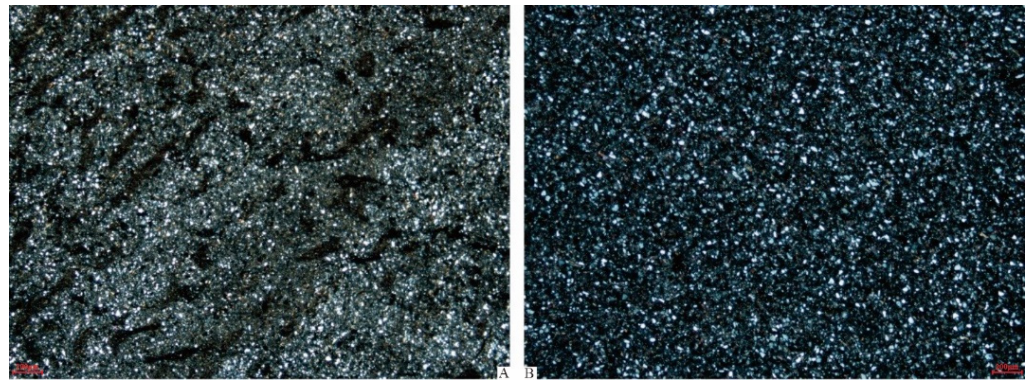


Figure 14. Microscopic photos of the rocks of the Shaqiaomu Formation ((A): Mudstone, (B): Siltstone).

These layers are organized into several basic sequences (Figure 15).

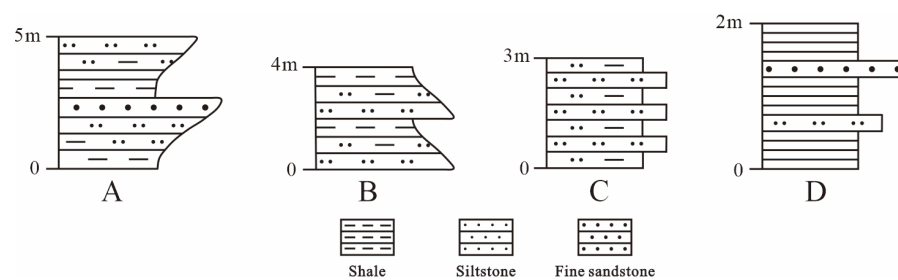


Figure 15. Stratigraphic sequence of the Shaqiaomu formation. A, B, C, D are type A, type B, type C, type D respectively.

Type A: The gray-black sandstone and mudstone interbedded output are characterized by a bottom layer of mudstone, which transitions upward into muddy siltstone and siltstone. The top of the sequence occasionally contains dark purple-red fine sandstone, forming a lower fine and upper coarse inverse grain sequence. The sandstone features groove molds and gouge erosion marks, with a high quartz content, generally exceeding 90%. Both the compositional maturity and structural maturity are high, indicative of a typical subtidal, near-coastal zone sand dam deposition (Figure 16). This type of basic sequence is predominantly found in layers 31 to 32 at the bottom of the section.

Type B: The lithology primarily comprises light gray siltstone, mud siltstone, and mudstone in unequally thick interbedded layers. The sequence typically begins with light gray siltstone at the bottom, transitioning upward to mud siltstone and mudstone, exhibiting a positive granular sequence structure. The sandstone bottom interface displays an abrupt lithological surface. This type is commonly observed in layers 36–39 and 45–46 of the section.

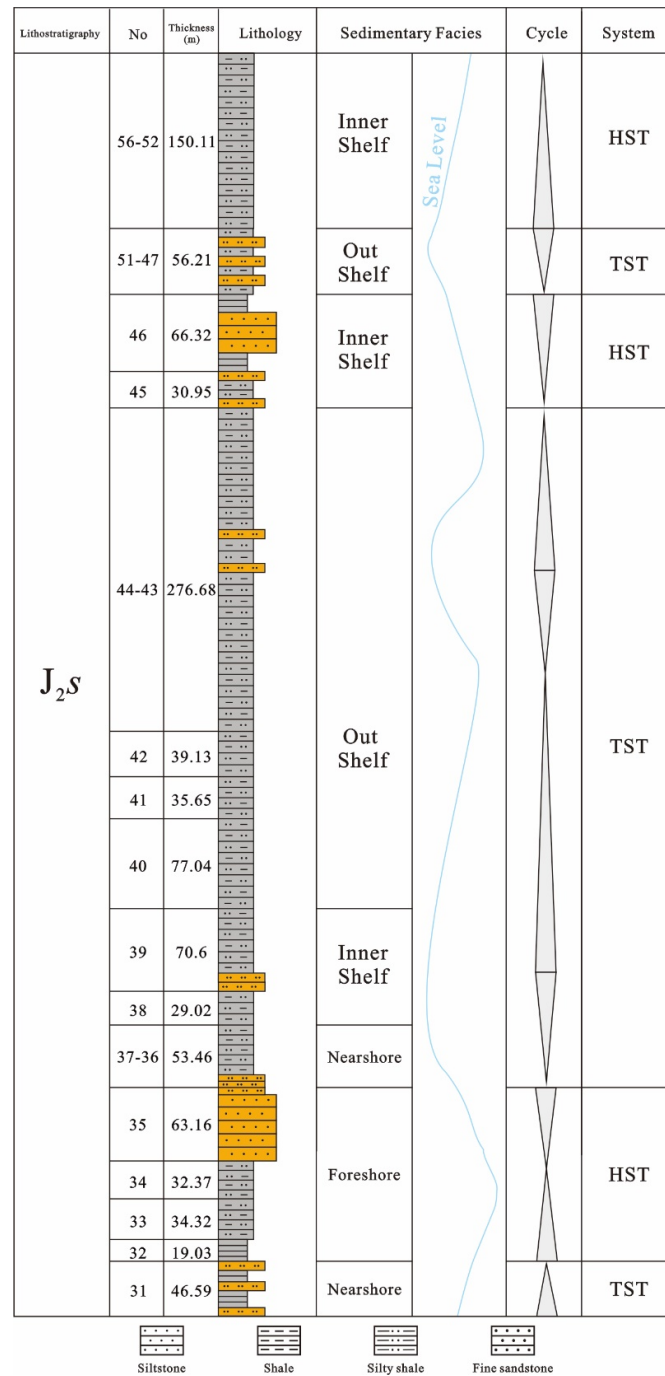


Figure 16. Sedimentary facies of the Shaqiaomu formation. Sandstone is uniformly filled in yellow, and carbonate rock is uniformly filled in cyan.

Type C: Yellow-green and purplish red siltstone interbedded with unequal thicknesses of siltstone, present a general sand-to-mud ratio of 1:1. These layers are predominantly thin, with single-layer thicknesses varying from 5 to 10 cm. Locally, the sand and mudstone exhibit oxidized shades of purplish red and yellow-brown, indicating a position above the redox interface and representing an inland shed depositional environment. This type of basic sequence is primarily developed in layers 52–56 at the top of the section.

Type D: The lithology mainly consists of gray-black shale, occasionally interspersed with dark red, thinly laminated siltstone and fine sandstone. The sandstone layers range from 5 to 15 cm in thickness, and local development of sand grain laminations and parallel laminations can be observed. The presence of a large amount of fine-grained muddy

sediments suggests a deeper water environment, representing an outer shelf depositional environment. This basic sequence is primarily found in layers 40 to 44 and 47 to 51 of the section.

The before-mentioned types of basic sequences share common features, such as progressively shallower water bodies, coarser grains, and thicker upward rock layers. These characteristics collectively form a distinct wave-dynamic dominated rhythmic layer within the shoreline–shelf sedimentary system.

5.4. Buqu Formation (J_2b)

The revised stratigraphic section of the Buqu Formation, located at Migaiertuoba (MP) on the southern flank of the Dongbula Backbone, presents two distinct types of basic stratigraphic sequences, as illustrated in Figure 17.

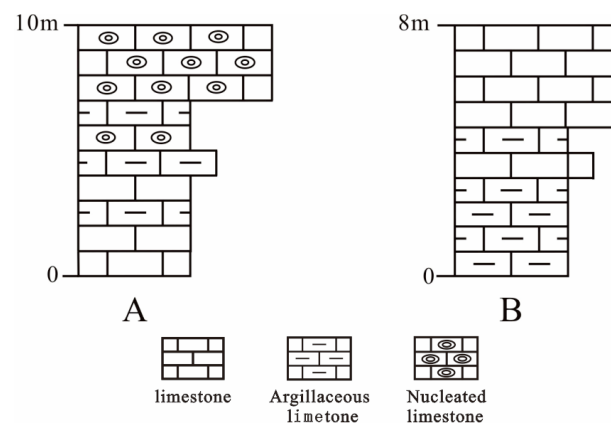


Figure 17. Stratigraphic sequence of the Buqu formation. A, B are type A and type B.

In the measured stratigraphic section, layers 1 through 14 primarily consist of unequally thick interbedded oncolitic limestone (Figure 18A) and marl (Figure 18B), with the fundamental sequence depicted in Figure 17A. The lower portion of the sequence typically features thinly to moderately bedded microcrystalline tuff interbedded with thinly bedded marl. In contrast, the upper portion is characterized by moderately thickly bedded oncolitic limestone, exhibiting an abrupt contact between the upper and lower units. The microcrystalline tuff at the base is generally light gray and possesses a microcrystalline structure. Under microscopic examination, a small amount of bioclastic material is visible, generally ranging from 1% to 5%. This bioclastic debris is predominantly composed of mesozoans, brachiopods, bivalves, coral, and echinoderm bioclastic debris, featuring small grain sizes, usually less than 2 mm, which represent ex situ transport deposits. The marl is typically dark gray, thinly laminated, and characterized by high mud content and negative topography due to weathering.

The upper oncolitic limestone is generally dark gray, moderately thickly laminated, and exhibits thickness variations between 30 and 50 cm within individual layers. Comprising 60% to 70% oncolitic stone size, this limestone is more uniformly distributed, with grain sizes ranging from 7.00 to 5.00 mm and poor sorting. This basic sequence type is developed at the base of the section, and four basic sequences of this type are visible vertically, exhibiting varying thicknesses. The presence of oncolitic limestone signifies an intertidal low-energy beach depositional environment. In contrast, the base contains a combination of bioclastic microcrystalline tuff and marl with low clastic content and fine, broken fragments, representing a subtidal low-energy environment characterized by low hydrodynamic conditions. This basic sequence type primarily develops in intertidal to subtidal environments and is characterized by the shallowing, coarsening, and thickening of grains and lithologies in correlation with the environment.

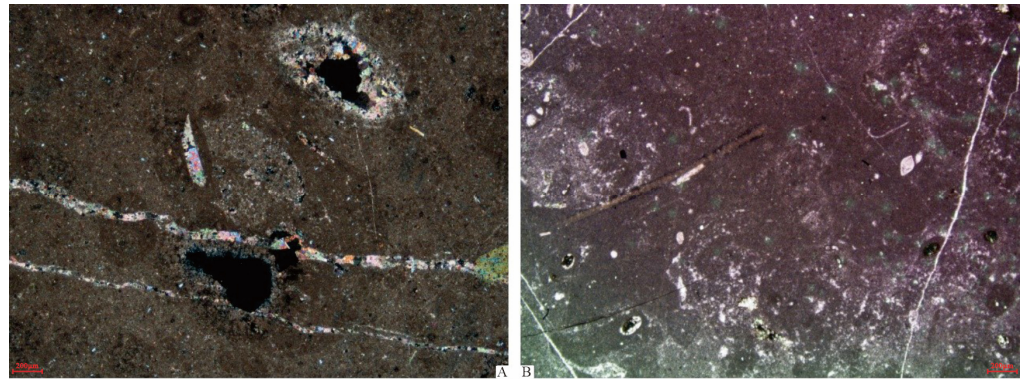



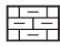
Figure 18. Microscopic photos of the rocks of the Buqu Formation ((A): Oncolitic limestone, (B): Microcrystalline limestone).

The upper section, comprising layers 15 to 22, primarily consists of unequally thick interbedded marl and marl crystalline tuff (Figure 19). The lower part of the sedimentary cycle is predominantly marl, which tapers upward to marl crystal tuff. These layers exhibit a combination of lower thickness and upper thinness in a ratio of 10:1 to 15:1 and terminate at the top with a petrographic abrupt interface. The marl is typically pale gray, possessing a grass-green weathering surface, a muddy structure, and thin laminae. With thicknesses generally ranging from 5 to 10 cm, the marl is easily weathered into negative stratigraphy, resulting in poor outcrop exposure. This geomorphology is orthogonal.

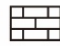
Lithostratigraphy	No	Thickness (m)	Lithology	Sedimentary Facies	Cycle	System
J ₂ x	22	40.01	[Limestone pattern]	Tidal Zone	HST	
	21	7.85	[Marl pattern]	Subtidal Zone		
	20	5.48	[Marl pattern]	Tidal Zone		
	19	23.27	[Marl pattern]	Subtidal Zone		
	18	11.63	[Marl pattern]	Tidal Zone		
	17	21.12	[Marl pattern]	Subtidal Zone		
	16	12.18	[Marl pattern]	Tidal Zone		
	15	16.69	[Marl pattern]	Subtidal Zone		
	14	20.66	[Marl pattern]	Tidal Zone		
	13	9.31	[Marl pattern]	Subtidal Zone		
	12	7.44	[Marl pattern]	Tidal Zone		
	11	16.13	[Marl pattern]	Subtidal Zone		
	10	7.4	[Marl pattern]	Tidal Zone		
	9	8.52	[Marl pattern]	Subtidal Zone		
	8	8.15	[Marl pattern]	Tidal Zone		
	7	15.56	[Marl pattern]	Subtidal Zone		
	6	26.33	[Marl pattern]	Tidal Zone		
	5	19.07	[Marl pattern]	Subtidal Zone		
	4	21.68	[Marl pattern]	Tidal Zone		
	3	13.08	[Marl pattern]	Subtidal Zone		
	2	15.25	[Marl pattern]	Tidal Zone		
	1	15.25	[Marl pattern]	Subtidal Zone		
					TST	



Oncolitic limestone



Argillaceous limestone



limestone

Figure 19. Sedimentary facies of the Buqu formation. Sandstone is uniformly filled in yellow, and carbonate rock is uniformly filled in cyan.

This pattern of negative marl topography in the lower sequence and positive marl topography in the upper sequence characterizes the upper stratigraphic development in the measured stratigraphic section of the Buqu Formation. Four basic sequences of varying thickness are visible vertically, each representing this type of stratigraphy. The marl at the base, thinly bedded and containing high mud and graywacke content, signifies a subtidal low-energy environment. In contrast, the marl at the top, which includes a small amount of oil-rich fractured biotite, can be interpreted as an intertidal depositional environment with strong hydrodynamic conditions.

Throughout the section, a total of eight “ash–mudstone” lithotrophic units can be identified, and two large sets of lithotrophic units (upper and lower lithotrophs) are distinguishable. The lower part consists of four rock units, composed of upper core limestone and lower marl intercalated with calcareous mudstone. These units exhibit a synclinal relationship between the “core limestone and marl” units. The genesis mechanism involves the formation of “transient inundation” during periodic environmental deepening, resulting in the creation of subtidal to semi-pelagic marls and calcareous mud shales in the lower part. Environmental shallowing leads to the formation of hydrodynamic upper parts within intertidal high-energy zones.

The upper part of the cyclonic unit consists of four rock cyclonic units, with the cyclonic unit itself comprising the upper microcrystalline tuff and the lower marl exposed in layers 15–22. As the marl content increases upward, the microcrystalline tuff layer’s thickness gradually decreases, becoming locally lenticular. The ratio of tuff to mud ranges from 10:1 to 15:1, and the contact between the cyclonic unit “tuff and mudstone” is gradual. From bottom to top, the unit is characterized by a progressively shallower environment, thinner rock layers, and finer and fewer grains, contrasting with the subtidal me-level spiral forming a typical positive grain order phase sequence. The genesis mechanism does not involve transient inundation during environmental deepening but rather the formation of normal shallow marine deposits. The process of environmental shallowing can lead to shallow exposure, resulting in thinly bedded muddy tuffs or even dolomitized tuffs, known as the “circumtidal ping–type meter–scale gyre” in the Meimeixiang phase [22].

Of the eight ash–mudstone cyclic sequences observed in the Buqu Formation, the bottom four represent typical carbonate subtidal meter-scale cycles, while the top four are characteristic of carbonate circumtidal meter-scale cycles. Carbonate sedimentation, which is primarily governed by accretion, exhibits heightened sensitivity to the deepening and shallowing effects of high-frequency sea-level fluctuations. This often results in the formation of upward shallowing sequences within the stratigraphic record, ranging from several tens of centimeters to a few meters in thickness. Anderson (1985) and Goodwin (1990) initially referred to this phenomenon as “meter–scale spallation.” [29,30]. It is primarily characterized by the general upward shallowing of the environment, and its causal mechanism stems from the periodic deepening and shallowing of the environment. This is geomorphologically characterized by alternating positive and negative topographic intervals.

During the Bathonian period, limestone deposition was common in the European Alps, especially in shallow marine environments. These limestones often contain abundant fossils, including ammonites, brachiopods, and corals [31].

5.5. Xiali Formation (J_2x)

The stratigraphy of the upper part is controlled by the Rugumiqiong section (RP) and the lower part by the Dongbula section (DP), with marker layers connecting the two sections. The stratigraphy exhibits clear vertical lithological segmentation. The lower segment (layers 06 to 21 in the DP section and layers 21 to 20 in the RP section) mainly consists of gray-green, dark black, and light gray shales, interbedded with bioclastic tuffs and muddy siltstones. Numerous chrysolitic and bivalve fossils are visible within the mudstones. The upper segment (layers 1 to 19 in the RP section) predominantly features yellow-gray and light gray siltstones and fine sandstones, locally interspersed with gray-

green calcareous shale, siltstone mudstone, gray-black mesoscopic tuff, and oolitic tuff. Two main types of basic sequences can be observed at the base (layers 06–21 in the DP section and layers 21–20 in the RP section):

Type A: This lithology primarily consists of light gray and yellow-gray mudstone and shale, interbedded with thin to medium-bedded yellow-gray marl and bioclastic tuff (Figure 20A). Locally, thin yellow-gray bedded muddy siltstone layers are also present. Bivalve, chrysolite, and brachiopod fossils are mostly preserved in thin layers, with a few crawling traces observed. A large number of fine-grained muddy deposits, along with an abundance of bivalve, gastropod, and chrysopod fossils and fossil remains, indicate a well-preserved outer shelf depositional environment that may have been deeper than the water column.

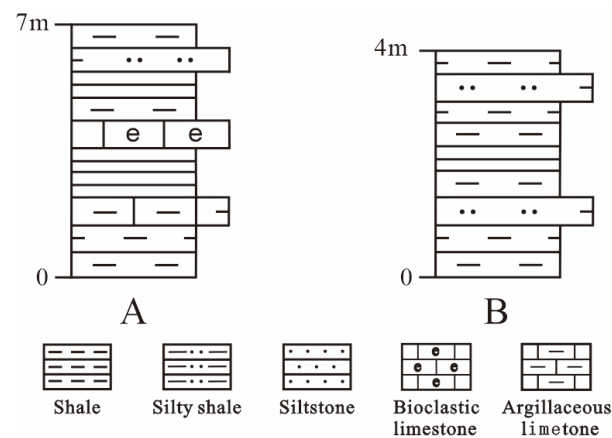


Figure 20. Stratigraphic sequence of the upper part of the Xiali formation. A,B are type A and type B.

Type B: Dark black and gray-green mudstones are intercalated with thinly bedded fine sandstones and muddy siltstones. The mudstone generally exhibits dark gray, gray-green, and dark black hues, with phyllite and very thin laminated output. Locally, it is interspersed with thinly laminated fine sandstone (Figure 21A) and muddy siltstone (Figure 21B), and the thickness of a single layer generally ranges from 5 to 10 cm. The thinly laminated sandstone layer represents storm sand layers formed during intense storm periods. This type of basic sequence signifies an inland shed depositional environment below the wave base surface and above the storm wave base surface. It can be found in layers 6 to 9 and 19 to 21 of the DP section. Layers 19 to 21 and RP19 to 20 are commonly developed (Figure 20B).

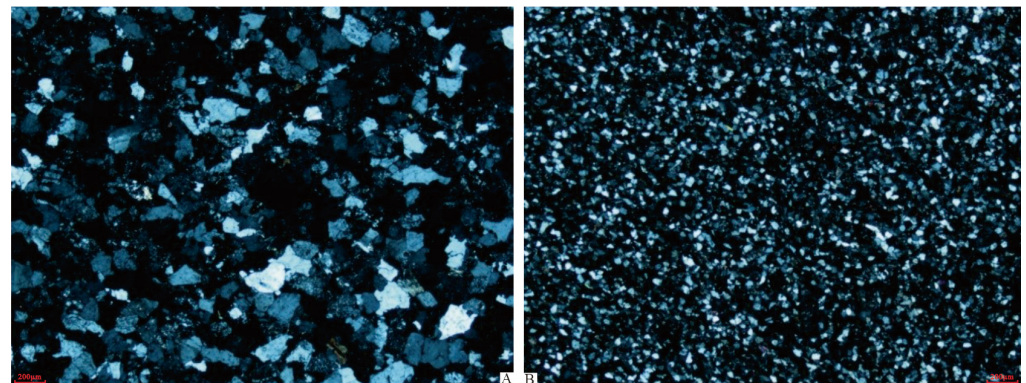


Figure 21. Microscopic photos of the rocks of the upper part of the Xiali formation ((A): Feldspar quartz sandstone, (B): Siltstone).

Five main types of basic stratigraphic sequences (Figure 22) are primarily developed in the top layers (layers 1 to 19 in the RP section).

Type A: The lithology mainly consists of yellow-gray and light gray muddy siltstone, accompanied by gray-green and light gray medium and coarse-grained sandstone, as well as fine sandstone. The bottom of the sequence typically comprises siltstone, muddy siltstone, and thinly laminated output, with single-layer thicknesses generally ranging from 5 to 10 cm. The sequence grades upward to medium-laminated medium and coarse-grained sandstone, which is typically medium-laminated output with single-layer thicknesses between 15 and 25 cm. Vertically, the sequence forms an upward coarsening and thickening inverse grain sequence. The sandstones are well-sorted and display low-angle flushing laminae and parallel laminae, representing a high hydrodynamic intertidal foreshore depositional environment situated between the high and low tide lines. In this environment, sediments are repeatedly flushed by tidal currents, forming parallel laminae and flushing laminae.

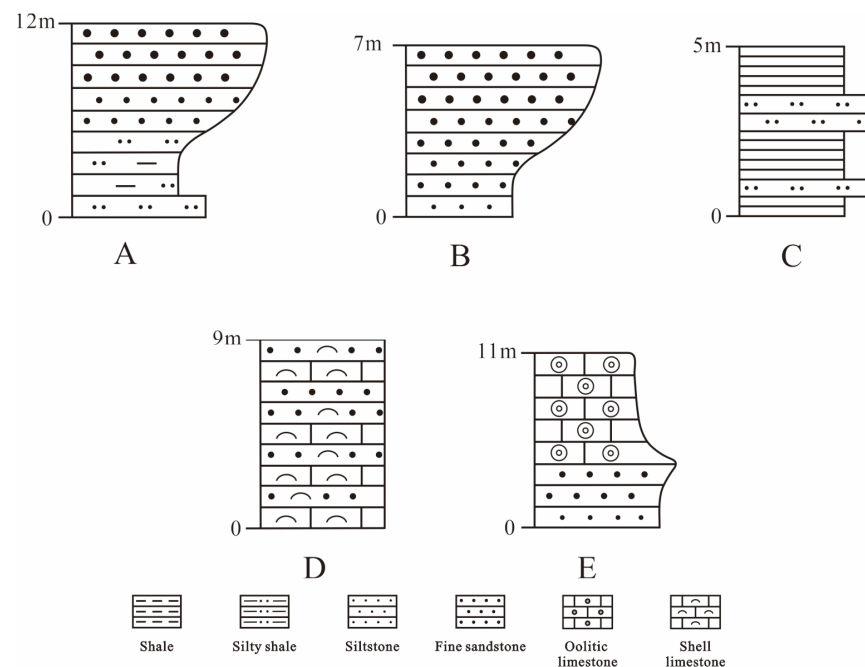


Figure 22. Stratigraphic sequence of the lower part of the Xiali formation. A, B, C, D, E are type A, type B, type C, type D and type E respectively.

Type B: The lithology closely resembles that of Type A, featuring gray-green medium to coarse-grained sandstone (Figure 23A) and fine sandstone. The bottom of the sequence generally consists of medium to fine-grained sandstone with thin bedding and a single-layer thickness between 3 and 6 cm. The sequence tapers upward to coarse sandstone, medium-to-thick bedded, with single-layer thicknesses typically between 10 and 30 cm. Parallel laminations and small sand laminations develop in the sandstone, which is well-sorted and contains heavy minerals. The development of sand laminations may suggest that the water column was deeper than in Type A. The sand barriers are generally deposited in the subtidal sublittoral zone, and this type of lamination is extensively developed in layers 5 to 8, 13, 14, 16, and 18 of the RP section.

Type C: Gray-green calcareous shale is interbedded with thinly laminated gray-green siltstone. The abundance of gray-green shale represents a pelagic hydrostatic environment and can be interpreted as a nearshore lower part close to a shelf depositional environment. Layers 9 and 19 of the RP section belong to this type of basic sequence.

Type D: The lithology primarily comprises gray-black oolitic limestone (Figure 23B) interbedded with oolitic sandstone, which is all thinly bedded. Single-layer thickness ranges from 8 to 15 cm, and the size of the oolitic shells varies from 5 to 2 cm. The content is generally above 70%, with good preservation and mostly occurring in parallel layers. This sequence should be deposited as sand barriers and oolitic beaches in the subtidal sublittoral zone.

Type E: This lithology is primarily characterized by gray-green oolitic tuffs, accompanied by gray-green medium- and fine-grained sandstones at the base, representing the sub-tidal sublittoral oolitic beach phase deposits.

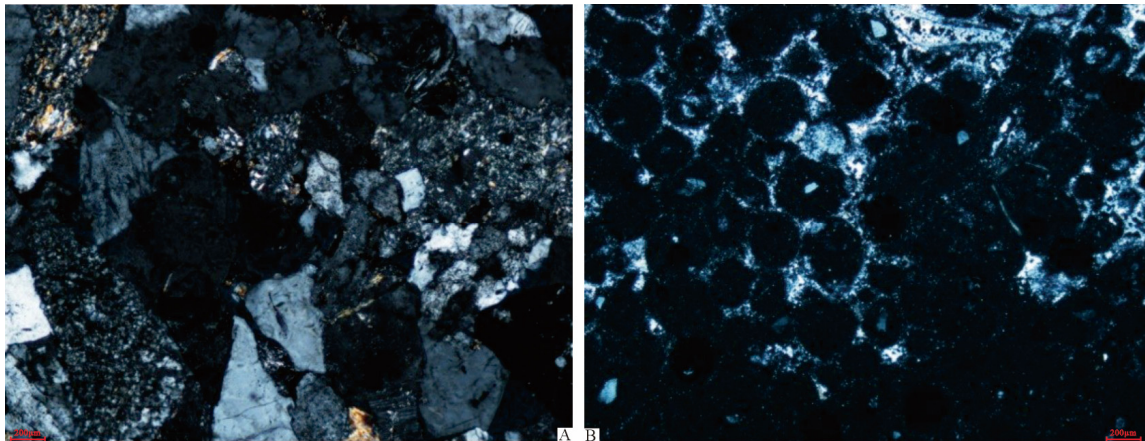


Figure 23. Microscopic photos of the rocks of the lower part of the Xiali formation ((A): Debris sandstone, (B): Oolitic limestone).

In the vertical direction, the Xiali Formation experienced a sedimentary evolutionary sequence transitioning from shelf-phase shale to shore-phase sandstone (Figure 24). This sequence exhibits a shallow depositional environment and a sandy-accreted coastal sedimentary sequence. Several rhyolitic layers, with thicknesses ranging from tens of centimeters to approximately 1 to 2 m, were developed within this sequence. These rhyolitic layers are characterized by a series of hair-grain rock sequences, resulting from the deepening of the water column during high-frequency sea-level changes. Conversely, the shallowing of the shoreline during high-frequency sea-level changes leads to the accretion of coastal sand bodies and the formation of coarser lithological units in the upper part.

5.6. Suowa Formation (J_3s)

In the Rugumiqiong section, the sediments of the Suowa Formation primarily consist of grain-supported carbonates (oncolitic limestones, oolitic tuffs, bioclastic tuffs) interspersed with minor ash-supported mud-crystal tuffs, bioclastic-bearing mud-crystal tuffs, and marls. The cement is predominantly mud-brilliant crystalline calcite, while the granular material is dominated by oolites, oncolitic rocks, and bioclasts, with a minor presence of land-derived clastic particles. The sediments are typically gray, exhibiting medium-to-thick layers and stable sediment thicknesses laterally.

The sediment characteristics suggest that the depositional environment of this formation includes more terrestrial mixing, implying that the depositional area is relatively close to the source area. The widespread occurrence of oolites, nucleolites, sandy debris, and biological debris indicates high hydrodynamic conditions, with the overall depositional characteristics of oolite and nucleolite beaches in the open terrace phase. Two main types of basic sequences are observed (Figure 25).

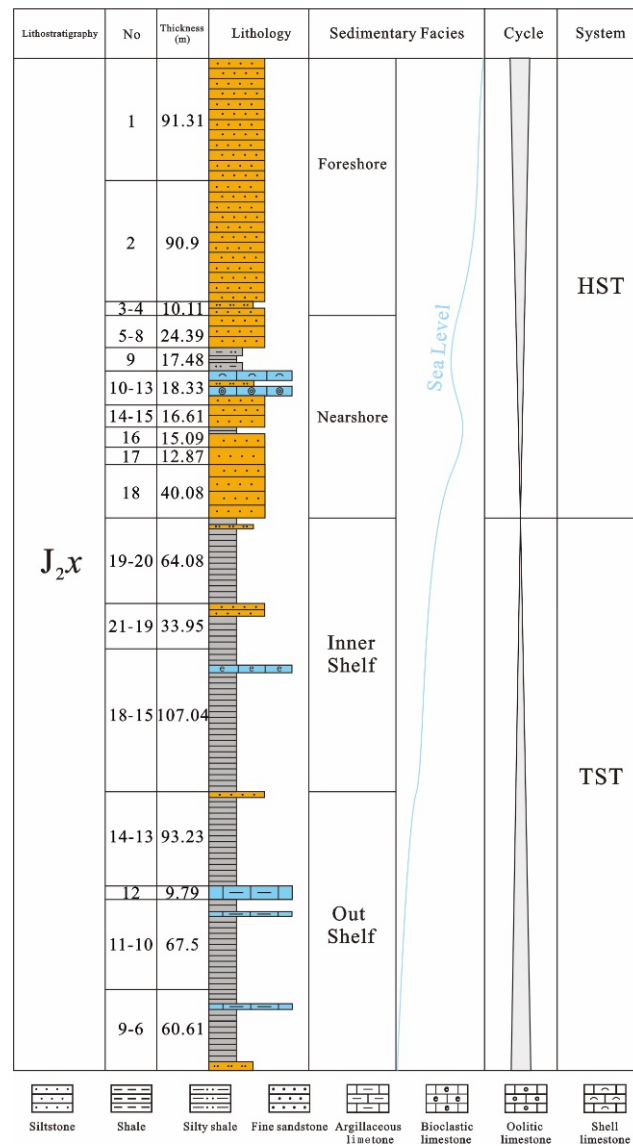


Figure 24. Sedimentary facies of the Xiali formation. Sandstone is uniformly filled in yellow, and carbonate rock is uniformly filled in cyan.

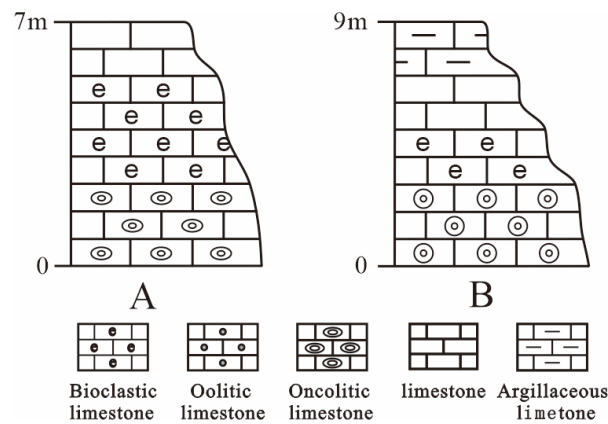


Figure 25. Stratigraphic sequence of the Suowa formation. A, B are type A and type B.

Type A: The lithology is primarily composed of dark black oncolitic limestone (Figure 26A,B), bioclastic limestone, and mud crystal limestone, with oncolitic limestone

being the most prominent feature. The grain types include bioclastic, oncolitic stone, and agglomerate, with a grain content generally exceeding 80%. The oncolitic stone grain is substantial, with the largest observable grains spanning several centimeters. The rock is mostly thick laminated, with scour surfaces visible locally. Above the scour surface, bioclastic and oncolitic stones fill the area, exhibiting a positive grain order in the vertical direction structure. The coarse-grained oncolitic limestone at the base is a product of the higher energy environment of the lower part of the subtidal platform, while the reduced bioclastic and oncolitic stone content of the upper part represents a lower dynamic condition of the water column and may be the product of deposition at lower sea level. This type is extensively developed in the section.

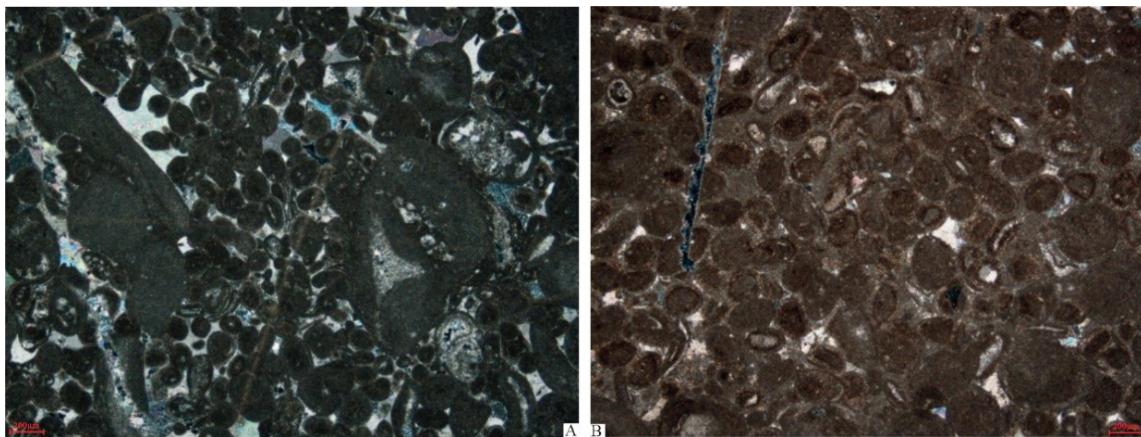


Figure 26. Microscopic photos of the rocks of the Suowa formation ((A): Nucleated limestone, (B): Nucleated limestone).

Type B: The lithology primarily consists of dark black oolitic tuffs, bioclastic oolitic tuffs, and mud crystal tuffs. The base is characterized by gray-black medium-to-thick bedded oolitic tuffs, which taper upwards to bioclastic oolitic tuffs and mud crystal tuffs. The bioclastic component is dominated by bivalve clasts, with a few gastropods and brachiopods, and its content varies from 10% to 40%. An apparent positive grain order structure is observed, and the grain size of the oolitic grains tends to become smaller upwards, while the bioclastic content gradually increases. This basic sequence is also widespread in the Sova Formation, indicating a product of the shallow water turbulent environment of the subtidal high-energy zone (Figure 27). The top marl is also a product of the sea-level fall.

According to regional data and stratigraphic distribution in the South Qiangtang basin, the vertical superposition relationship and spatial spreading characteristics of petrographic types in the section suggest that the Jurassic deposition period was primarily characterized by shallow water deposition on a land shelf. The environment predominantly consisted of a mixed carbonate and clastic rock terrace. The overall paleogeographic background was deeper in the south and shallower in the north, with coarser grain size in the north and finer grain size in the south. This trend can be roughly traced along a line from Sewa to Zigetangcuo to Anduo.

Using this line as a boundary, the southern side primarily constituted the central sedimentary area of the basin, where a series of gray and black mud shale and marl deep-water deposits were formed. Conversely, the northern side mainly featured shallow water terrace deposits, which consisted of shelf-coastal phase sand mudstone and shallow marine carbonate rocks. The sedimentary facies of the Oxfordian period in the Alps are mainly carbonate rocks that formed in different depositional environments, such as evaporative platform, restricted platform, open platform, reef-shoal complex, bioclastic shoal, bioherm, and intershoal. Some of the fossils that have been found in the Oxfordian rocks include ammonites, marine reptiles, and bivalves. Some of the specific names of the

fossils are *Brightia thuouxensis*, *Pictonia baylei*, *Epipeltoceras bimammatum*, *Perisphinctes bifurcatus*, *Gregoryceras transversarium*, *Perisphinctes plicatilis*, *Cardioceras cordatum*, and *Quenstedtoceras mariae* [31,32].

Lithostratigraphy	No	Thickness (m)	Lithology	Sedimentary Facies	Cycle	System
J_3S	13	3		Subtidal Zone		TST
	12	15				
	11	12				
	10	8.5				
	9	3				
	8	8.5				
	7	5				
6	3.5					
5	2					
4	6					
3	2.8					
2	7.5					
1	2					

Bioclastic limestone Oolitic limestone Oncolitic limestone

Figure 27. Sedimentary facies of the Suowa formation.

From the Early Paleozoic to the Late Paleozoic, the sedimentary environment of the Qiangtang Block was characterized by stable coastal and shallow marine deposition. During the Triassic to Jurassic period, shallow marine clastic rocks and limestone were formed, while the Qiangtang Block was unconformably overlain by continental red beds during the Cretaceous period. The overall sedimentary environment of the Qiangtang Block from the Early Paleozoic to the Cretaceous exhibited a shallowing trend, which may be attributed to the gradual uplift of the relatively small Qiangtang Block as it rifted from the Gondwana supercontinent. This uplift occurred alongside the development of the Yanshan and Himalayan tectonic cycles within the Paleo-Tethys Ocean, causing the sedimentary environment to transition from marine to its present-day continental environment.

6. Conclusions

The present study offers a comprehensive analysis of the sedimentary evolution of the Jurassic period in the South Qiangtang Basin. In the South Qiangtang Basin, a progressive shallowing of the sedimentary environment has been observed, spanning from the Lower Jurassic Quse Formation to the Upper Jurassic Suowa Formation. This transition is marked by an evolution in sedimentary facies, shifting from the outer shelf to the subtidal zone. This trend can be attributed to the sequential geological events that occurred during the Late Triassic, Middle Jurassic, and Late Jurassic periods. These events include the splitting and expansion of the Bangong–Nujiang suture zone, subduction processes, and finally, plate movements that facilitated the suturing and splicing of the Qiangtang–Lhasa plate.

The decreasing trend of relative sea-level changes during the Jurassic period in the southern Qiangtang area contrasts with the rising trend observed in European sea-level changes, as studied by Hallam, Haq, and others. This discrepancy can be attributed to

the development of the Yanshan and Himalayan tectonic cycles, which led to the collision and welding of the Qiangtang Block with the northward-drifting Gangdese-Nyenchen Tanglha Block. As a result, the Bangong Lake–Nujiang Trench at the southern boundary of the Qiangtang Basin disappeared, and seawater retreated from east to west. Consequently, the Qiangtang region gradually emerged above water, marking the end of marine sedimentation.

Author Contributions: Conceptualization, Z.C. and Q.W.; Investigation, Z.C.; Writing—original draft, Z.C., H.Y. and Q.W.; Writing—review and editing, Z.C., H.Y. and Q.W. All authors have read and agreed to the published version of the manuscript.

Funding: This research was supported by Guangdong University of Petrochemical Technology (519013).

Data Availability Statement: The research created experimental data that can be found in the tables and figures presented in this manuscript.

Acknowledgments: In closing, we would like to express our profound gratitude to all the co-authors for their invaluable contributions to this paper. Their collective expertise, commitment, and collaboration have been the driving force behind the realization of this research project. We would also like to extend our heartfelt appreciation to the editor-in-chief of the journal, whose astute guidance and unwavering support have been instrumental in shaping this work. Furthermore, we are immensely grateful to the anonymous reviewers for their insightful comments, constructive criticism, and invaluable suggestions, which have significantly enhanced the quality and rigor of our manuscript. The collective efforts of these individuals have been integral to the success of this endeavor, and we are truly indebted to them for their time, expertise, and dedication.

Conflicts of Interest: The authors declare that they have no known competing financial interest or personal relationships that could have appeared to influence the work reported in this paper.

References

1. Xian, B.; Zhu, X.; Yue, D.; Zheng, X. Current hot topics and advances of sedimentology: A summary from 19th International Sedimentological Congress. *J. Palaeogeogr.* **2014**, *16*, 816–826.
2. Santantonio, M. Facies associations and evolution of pelagic carbonate platform/basin systems: Examples from the Italian Jurassic. *Sedimentology* **1993**, *40*, 1039–1067. [[CrossRef](#)]
3. Martire, L. Stratigraphy, facies and synsedimentary tectonics in the Jurassic Rosso Ammonitico Veronese (Altopiano di Asiago, NE Italy). *Facies* **1996**, *35*, 209–236. [[CrossRef](#)]
4. Basilone, L. Mesozoic tectono-sedimentary evolution of the Trapanese Southern Tethyan margin (NW Sicily) integrating facies and stratigraphic analysis with subsidence history. *Ital. J. Geosci.* **2020**, *139*, 54–75. [[CrossRef](#)]
5. Hallam, A. A review of the broad pattern of Jurassic sea-level changes and their possible causes in the light of current knowledge. *Palaeogeogr. Palaeoclimatol. Palaeoecol.* **2001**, *167*, 23–37. [[CrossRef](#)]
6. Carminati, E.; Doglioni, C. Alps vs. Apennines: The paradigm of a tectonically asymmetric Earth. *Earth-Sci. Rev.* **2012**, *112*, 67–96. [[CrossRef](#)]
7. Santantonio, M. General Field Trip Guidebook. In Proceedings of the 6th International Symposium on the Jurassic System, Palermo, Italy, 12–22 September 2002.
8. Martire, L.; Pavia, G. Jurassic sedimentary and tectonic processes at Montagna Grande (Trapanese Domain, Western Sicily, Italy). *Riv. Ital. Paleontol. E Stratigr.* **2004**, *110*, 23–34.
9. Basilone, L. Mesozoic tectono-sedimentary evolution of Rocca Busambra in western Sicily. *Facies* **2009**, *55*, 115–135. [[CrossRef](#)]
10. Yi, H.; Lin, J. New information on the stratigraphy of the Qiangtang basin in northern Tibet. *Geol. Rev.* **2003**, *49*, 59–65. (In Chinese)
11. Huang, J. Tectonic features and evolution of the Qiangtang Basin, northern Tibet. *Reg. Geol. China* **2001**, *20*, 178–186. (In Chinese)
12. Cai, L.; Dong, Y.S.; Zhai, Q.G.; Wang, L.Q.; Yan, Q.R.; Wu, Y.W.; He, T.T. Zircon SHRIMP dating of early Paleozoic ophiolite—Stacked crystal gabbro from Qiangtang, Qinghai-Tibet Plateau and its significance. *J. Petrol.* **2008**, *24*, 31–36. (In Chinese)
13. Zhai, Q.G.; Li, C.; Wang, J.; Chen, W.; Zhang, Y. Petrology, mineralogy and (40)Ar/(39)Ar chronology of blue schist in the Jompa area, central Qiangtang, northern Tibet. *J. Petrol.* **2009**, *25*, 2281–2288. (In Chinese)
14. Zhai, Q.G.; Wang, J.; Cai, L.; Su, L. Zircon SHRIMP chronology and Hf isotopic signatures of Middle Ordovician metamorphic pile crystal gabbro from central Qiangtang, Qinghai-Tibet Plateau. Chinese Science. *Earth Sci.* **2010**, *40*, 565–573. (In Chinese)
15. Dong, Y.S.; Zhang, X.Z.; Shi, J.R.; Wang, S.Y. Petrological and metamorphic characteristics of garnet dolomite schist in the central Qiangtang high-pressure metamorphic belt, northern Tibet. *Geol. Bull.* **2009**, *28*, 1201–1206. (In Chinese)
16. Yanwang, W. Longmuco-Shuanghu-Lancangjiang Ocean Historical Record of Cambrian-Permian Ophiolites. Ph.D. Thesis, Jilin University, Jilin, China, 2013.

17. Cai, L. The Longmucuo-Shuanghu-Lancangjiang plate suture zone and the Carboniferous Permian Gondwana northern boundary. *J. Chang. Geol. Inst.* **1987**, *155–166*. (In Chinese)
18. Cai, L.; Tianwu, W. Material composition and tectonic evolution of the Qiangtang Central Uplift, Tibet. *J. Chang. Univ. Sci. Technol.* **2001**, *25–31, 36*. (In Chinese)
19. Cai, L.; Zhai, Q.G.; Dong, Y.S.; Zeng, Q.G.; Huang, X.P. Evolutionary record of the Longmucuo-Shuanghu plate suture zone and Qiangtang Paleotethys Ocean on the Qinghai-Tibet Plateau. *Geol. Bull.* **2007**, *1*, 13–21. (In Chinese)
20. Cai, L. Twenty years of research on the Longmucuo-Shuanghu-Lancang River plate suture zone on the Qinghai-Tibet Plateau. *Geol. Rev.* **2008**, *54*, 105–119. (In Chinese)
21. Li, C.; Zhai, G.; Wang, L.; Yin, F.G. An important window for understanding the Tibetan Plateau: A review of recent research progress in the Qiangtang region. *Geol. Bull.* **2009**, *28*, 1169–1177. (In Chinese)
22. Wang, Z.J.; Wang, J.; Yin, F.G.; Chen, M. Sedimentary-tectonic transformation and hydrocarbon source rocks in the Jurassic basin of South Qiangtang. *Geol. China* **2007**, *33*, 1285–1291. (In Chinese)
23. Geng, Q.R.; Pang, G.T.; Wang, L.Q.; Peng, Z.M.; Zhang, Z. Geological background of Tethys evolution and mineralization in the Qiangtang Massif, Bangong Lake-Nujiang Belt. *Geol. Bull.* **2011**, *31*, 1261–1274. (In Chinese)
24. Wang, J.; Fu, X.; Wei, H.; Shen, L.; Wang, Z.; Li, K. Late Triassic basin inversion of the Qiangtang Basin in northern Tibet: Implications for the closure of the Paleo-Tethys and expansion of the Neo-Tethys. *J. Asian Earth Sci.* **2022**, *227*, 105–119. [[CrossRef](#)]
25. Zheng, Z.Y.; Zuo, Y.H.; Wen, H.G.; Li, D.M.; Luo, Y.; Zhang, J.Z.; Yang, M.H.; Zeng, J.C. Natural gas characteristics and gas-source comparisons of the lower Triassic Feixianguan formation, Eastern Sichuan basin. *Pet. Sci.* **2023**. [[CrossRef](#)]
26. Zheng, Z.Y.; Zuo, Y.H.; Wen, H.G.; Zhang, J.Z.; Zhou, G.; Xu, L.; Sun, H.F.; Yang, M.H.; Yan, K.N.; Zeng, J.C. Natural gas characteristics and gas-source comparisons of the Lower Triassic Jialingjiang Formation, Eastern Sichuan Basin. *J. Pet. Sci. Eng.* **2022**, *221*, 111165. [[CrossRef](#)]
27. Carol Marie, T. Toarcian Stage. In *Encyclopedia Britannica*; Encyclopædia Britannica, Inc.: Chicago, IL, USA, 2013.
28. Gawlick, H.J.; Missoni, S. Middle-Late Jurassic sedimentary mélange formation related to ophiolite obduction in the Alpine-Carpathian-Dinaridic Mountain Range. *Gondwana Res.* **2019**, *74*, 144–172. [[CrossRef](#)]
29. Mei, M.; Xu, D.; Zhou, H. Genetic Types of Meter-Scale Cyclic Sequences and Their Fabric Features of Facies-Succession. *Acta Sedimentol. Sin.* **2000**, *18*, 43–49. (In Chinese)
30. Anderson, E.J.; Goodwin, P.W. The significance of metre-scale allocycles in the quest for a fundamental stratigraphic unit. *J. Geol. Soc.* **1990**, *147*, 507–518. [[CrossRef](#)]
31. Corbin, J.C.; Person, A.; Iatzioura, A.; Ferre, B.; Renard, M. Manganese in pelagic carbonates: Indication of major tectonic events during the geodynamic evolution of a passive continental margin (the Jurassic European margin of the Tethys–Ligurian Sea). *Palaeogeogr. Palaeoclimatol. Palaeoecol.* **2000**, *156*, 123–138. [[CrossRef](#)]
32. Wu, Q.; Liu, Q.; Liu, S.; Wang, S.; Yu, J.; Ayers, W.B.; Zhu, Q. Estimating Reservoir Properties from 3D Seismic Attributes Using Simultaneous Prestack Inversion: A Case Study of Lufeng Oil Field, South China Sea. *SPE J.* **2022**, *27*, 292–306. [[CrossRef](#)]

Disclaimer/Publisher’s Note: The statements, opinions and data contained in all publications are solely those of the individual author(s) and contributor(s) and not of MDPI and/or the editor(s). MDPI and/or the editor(s) disclaim responsibility for any injury to people or property resulting from any ideas, methods, instructions or products referred to in the content.